

Photoluminescence and Photo-Catalytic Activity of Synthesized Nanocrystals

Mansi Chitkara, Khanesh Kumar, Sanjeev Kumar and I S Sandhu

Department of Applied Sciences, Chitkara University,
Rajpura 140 401, Punjab, India

E-mail: sanjeevkumar@chitkara.edu.in

Karamjit Singh

Department of Physics, Punjabi University,
Patiala 147 002, Punjab, India

Abstract

Intrinsic and extrinsic semiconductor nanostructures have attracted great attention due to their size tunable photo-physical and photo-chemical properties. In the present paper, polyvinyl pyrrolidone (PVP) capped $Zn_{1-x}Eu_xS$ ($0.00001 \leq x \leq 0.1$) nanocrystals have been synthesized by means of a facile chemical synthesis method. Crystallography and morphology of synthesized materials have been deliberated using X-ray diffraction (XRD) and transmission electron microscope (TEM), respectively. Diffraction and electron micrograph studies reveal that the synthesized materials are zinc blende nanocrystals having average particle size ~ 3 nm. Elemental and compositional analyses of the nanocrystals have been done using energy dispersive X-ray fluorescence (EDXRF) technique. Steady state photoluminescence spectra have been recorded for optical characterization of synthesized nanomaterials. Photo-catalytic activity potential of synthesized nanomaterials under UV radiation exposure has been investigated using methylene blue (MB) dye as a test contaminant in aqueous media. Photo-physical and photo-chemical behaviour dependence on doping concentration has been described in detail. Moreover, the sophistication of competition between charge carrier recombination and charge carrier trapping followed by the competition between recombination of trapped carriers and interfacial charge transfer processes have been presented in a fantastic and elaborative way by comparative study of photoluminescence and photo-catalytic activity results.

Keywords: Nanocrystals, Crystallography, Morphology, Photoluminescence, Photo-catalytic activity.

INTRODUCTION

Semiconductor nanocrystals consisting of hundreds to thousands of atoms have been prime area of research since last few decades [1-3]. Transition from bulk to nano size (< 100 nm) lead to extremely large surface area to volume ratio as well as quantum confinement effects [4-9]. The extremely enhanced surface to volume ratio of nanocrystals augments the chemical reaction dynamics and photon absorption efficiency. Semiconductor nanostructures exhibit strong size-dependent physical, chemical and optical

Journal on Today's Ideas -
Tomorrow's Technologies
Vol. 1, No. 1
June 2013
pp. 15–28



©2013 by Chitkara
University. All Rights
Reserved.

Chitkara, M.
Kumar, K.
Singh, K.
Kumar, S.
Sandhu, I. S.

16

properties with potential applications in the field of bio-imaging, opto-electronics as nanosensors, nanophosphors, nanophoto-catalyst, phototoconductors and laser materials. The increased public concern with environmental pollutants demands to develop a novel and economic treatment methods based on photo-catalysis reactions for pollutant degradation. Photo-catalysis is a photon induced catalytic process in which the photogenerated electron-hole pairs in a catalyst undergoes redox reactions with molecules adsorbed onto the surface, thereby breaking these into smaller fragments. Higher the effective surface area, higher will be the adsorption of target molecules leading to better photo-catalytic activity. Doping of semiconductor with suitable dopant creates quasi-stable energy states within the band gap, thereby affecting the optical and electronic properties. Increased electron trapping due to higher defect sites leads to enhancement in the photo-catalytic efficiency provided the electron-hole pair recombination rate is lower than the rate of electron transfer to adsorbed molecules.

Various new compounds and materials for photo-catalysis have been synthesized in the past few decades. Large number of experimental investigations [4, 10-13] on semiconductor nanomaterials have been mainly focused on wide bandgap II-VI compound semiconductors. Pure and doped ZnS nanocrystals have shown potential applications for environmental cleaning as well as fast & efficient nanophosphors. Semiconductor photo-catalysts with enhanced redox potential of conduction band electrons and valence band holes have been used for the complete elimination of toxic chemicals [14-15]. The wide scale use of TiO₂ for photo-catalytic activities under sunlight has been studied in detail by Martyanov et.al. [16]. ZnO, with a high surface reactivity due to a large number of native defect sites arising from oxygen non-stoichiometry, has emerged to be an efficient photo-catalyst material as compared to other metal-oxides [17-18]. One-dimensional nanostructures with high surface to volume ratio can be attractive candidates for photo-catalysis. Comparative results of photo-catalytic degradation studies of MB dye with visible light irradiation demonstrated that ZnO nanorods are 12–24% more active than nanoparticulate films [19]. There are reports on the enhancement of visible light absorption in ZnO by doping with Co [20], Mn [21], Pb and Ag [22], etc. Zheng et al. [23] correlated luminescence and photo-catalytic activity of ZnO nanocrystals with the intrinsic and extrinsic crystal defects. The dependence of photo-catalytic efficiency on optimal particle size of TiO₂ nanocrystallites has been studied by Wang et al. [24]. Choi et al. [25] reported a systematic study of the effects of various metal ion dopants on nanocrystalline TiO₂. High photo-catalytic activity of nanoporous ZnO nanoparticles have been reported by Hu et al. [26]. They found that the photo-catalytic activity of ZnO nanocrystals is mainly

dependent on the type and concentration of oxygen defects. Recently, Bang et al. [27] synthesized & analysed Ni²⁺ doped ZnS hollow microspheres and nanoparticles using ultrasonic spray pyrolysis.

ZnS nanocrystals doped with optical active luminescent centers create new opportunities in luminescence studies of doped semiconductor nanoclusters. Eu³⁺ doped ZnS nanocrystals are promising nanophosphors because these are chemically more stable as compared to other Eu³⁺ doped semiconductor chalcogenides. Luminescence efficiency of pure ZnS nanocrystals is substantially enhanced by doping with bivalent transition-metal ions as well as rare earth metal ions such as Cu²⁺, Mn²⁺, Sm²⁺ etc. [4, 10, 28]. Doping with rare-earth (RE) metal ions is not a simple method, as it requires specific preparation conditions. To the best of our knowledge only limited reports [29, 30] on the preparation of stable RE ion-doped II–VI compound semiconductor nanocrystals are available in literature. The present paper reports steady state photoluminescence and photo-catalytic activity potential of bottom-up grown Zn_{1-x}Eu_xS (0.00001 ≤ x ≤ 0.1) nanocrystals. Photo-catalytic activity has been well correlated with the luminescence quantum yield. Moreover, photo-catalytic and luminescence efficiency dependence on the Eu³⁺ concentration have been described in detail.

Experimental

PVP capped Zn_{1-x}Eu_xS (0.00001 ≤ x ≤ 0.1) nanocrystals have been synthesized using facile bottom-up synthesis approach; wet chemical co-precipitation method. Analytical reagent grade chemicals: zinc acetate (C₄H₆O₄Zn.2H₂O) (procured from Qualigens Fine Chemicals, Mumbai), sodium sulphide (Na₂S.xH₂O) (procured from Loba Chemie Pvt. Ltd. Mumbai), europium acetate hydrate [(C₂H₃O₂)₃Eu.xH₂O] (procured from Sigma-Aldrich, USA) and polyvinylpyrrolidone (PVP) (procured from HIMEDIA laboratories Pvt. Ltd. Mumbai) were used without further purification for nanocrystals synthesis. Aqueous solutions of 0.5M C₄H₆O₄Zn.2H₂O, 1M (C₂H₃O₂)₃Eu.xH₂O, 0.5M Na₂S.xH₂O and 2 % PVP were prepared in triple distilled water. Then precursor solutions alongwith PVP were mixed in stoichiometric proportion at room temperature under vigorous stirring. More details about the chemical co-precipitation method have been already described by Singh et. al [13]. The resulting precipitates were centrifuged and dried in vacuum oven for 10-12h continuously.

Panalytical's X'Pert Pro Powder XRD setup equipped with 3050/60 Goniometer and Cu anode X-ray tube has been used for crystallographic characterization of synthesized nanomaterials. Morphological characterization has been done using Hitachi (H-7500) TEM.

Chitkara, M.
Kumar, K.
Singh, K.
Kumar, S.
Sandhu, I. S.

The elemental and compositional analyses of the synthesized nanocrystals have been carried out using energy dispersive X-ray fluorescence (EDXRF) spectrometer involving Mo anode X-ray tube (PAN-Analytic) as an excitation source and LEGe (Canberra made, FWHM = 150 eV at 5.89 keV) photon detector.

Energy resolved luminescence spectra have been recorded using FlouoroMax-3 (Jobin-Yvon, Edison, NJ, USA) spectrofluorometer equipped with photomultiplier tube and a Xenon lamp.

The photo-catalytic activity of synthesized nanocrystals has been examined by studying the degradation of MB ($C_{16}H_{18}ClN_3S \cdot 2H_2O$) dye solution under UV-irradiation. A 350 ml of aqueous suspension was prepared by completely dissolving 1.1322 mg of the MB dye and then dispersing 140 mg of nanocrystals in the de-ionized water. The resulting suspension was equilibrated by stirring in the dark for 1 h to stabilize the adsorption of MB dye on the surface of nanocrystals. The stable aqueous suspension was then exposed to the UV-radiation with continuous magnetic stirring, using the home made photoreactor containing two 18-W tubes as the UV-source ($\lambda = 200\text{--}400$ nm). Following the UV-radiation exposure, 10 ml sample of aqueous suspension was taken out after every 10-min interval for the total 80 min of the UV-radiation exposure. The aqueous dye solution was examined using UV-vis absorption spectrophotometer (Systronics PC Based Double Beam Spectrophotometer:2202) to study the photo-degradation of the MB dye.

18

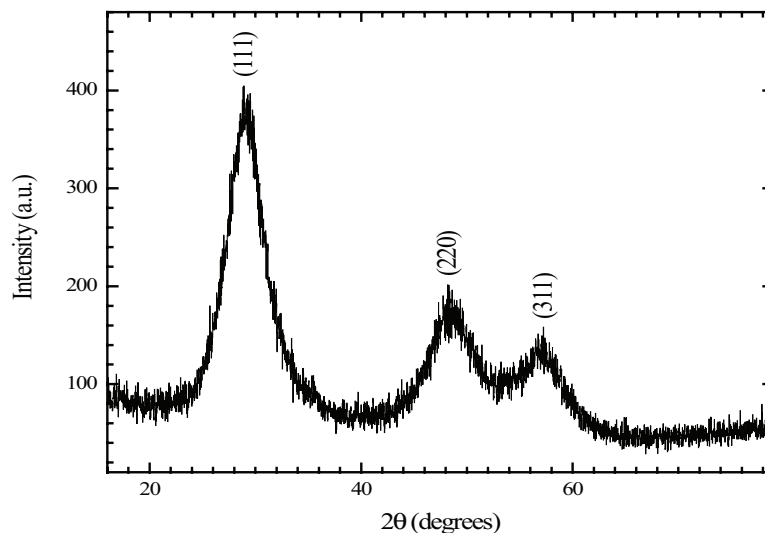


Figure 1: XRD pattern of $Zn_{0.90000}Eu_{0.10000}S$ nanocrystals.

Results and Discussion

Crystallographic and morphological studies

Powder X-ray diffraction patterns recorded for all the synthesized samples show peak broadening due to the presence of nanocrystallites, one such diffractogram has been shown in Fig. 1. Comparison of recorded diffraction patterns with standard JCPDS data files confirms that the synthesized material is zinc blende (cubic) ZnS with the planes {111}, {220}, and {311}, respectively. Moreover, the absence of any additional peak in the recorded XRD patterns rule out presence of any impurity phase. The average crystalline size calculated from recorded XRD patterns using Scherrer formula [31] is ~3nm .

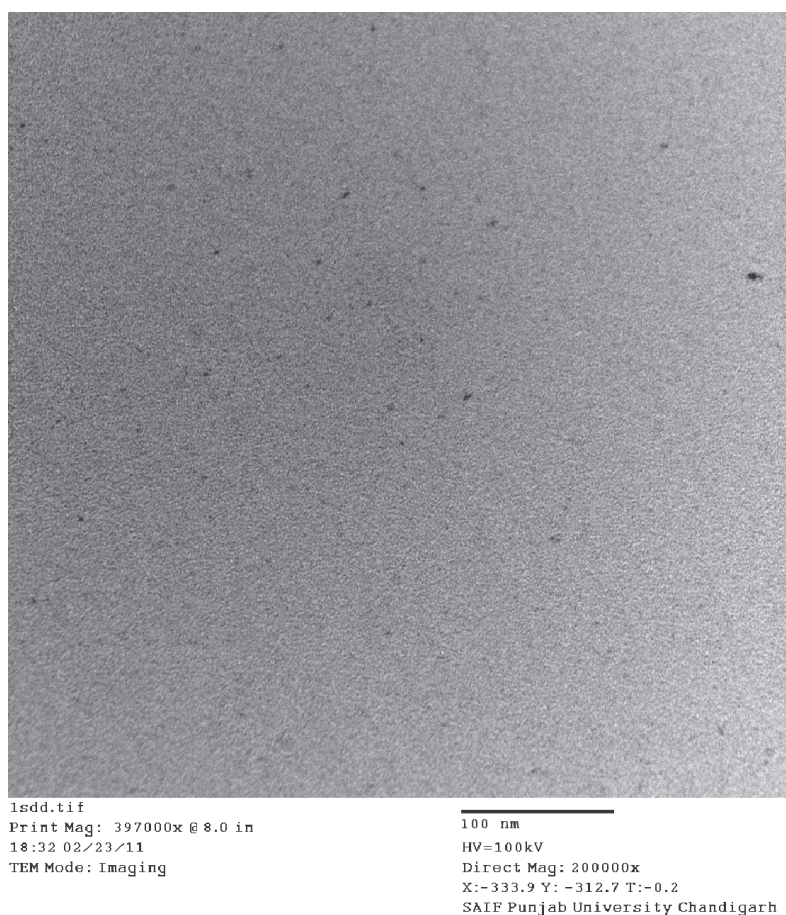


Figure 2: TEM micrographs of $Zn_{0.90000}Eu_{0.10000}S$ nanocrystals.

Chitkara, M.
Kumar, K.
Singh, K.
Kumar, S.
Sandhu, I. S.

Recorded TEM micrographs (Fig. 2) confirm formation of nearly monodisperse nanoparticles with average particle size $\sim 3\text{-}4$ nm. The average particle size calculated from electron micrographs is in close proximity with average crystalline size calculated from XRD. So, all the synthesized particles are single nanocrystals.

Elemental and compositional analysis using energy dispersive X-ray fluorescence (EDXRF) technique

20

The elemental and compositional analysis of synthesized $\text{Zn}_{1-x}\text{Eu}_x\text{S}$ ($0.0001 \leq x \leq 0.1$) nanocrystals have been performed using rapid, sensitive and non-destructive energy dispersive X-ray fluorescence (EDXRF) techniques. The EDXRF spectrometer involves a 2.4 kW Mo anode X-ray tube (Panalytic, Netherland) equipped with selective absorbers as an excitation source and a LGe detector (FWHM = 150 eV at 5.895 keV, Canberra, US) coupled with PC based multi-channel analyzer to collect the fluorescent X-ray spectra.

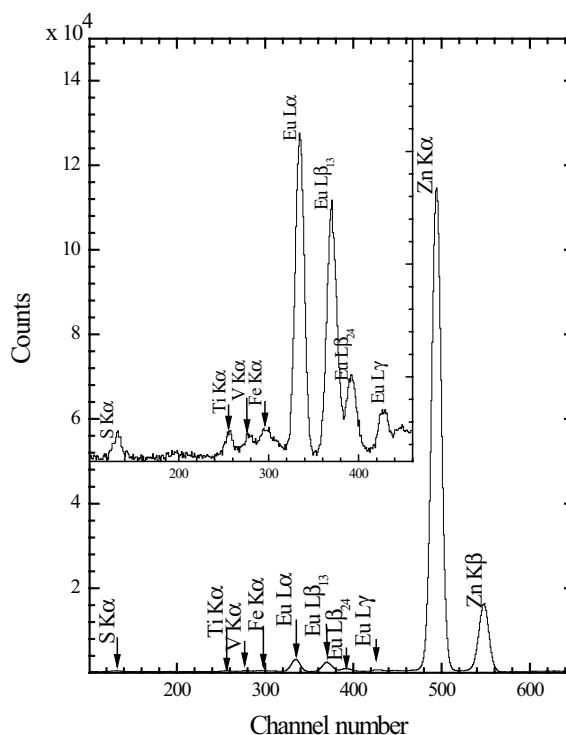


Figure 3: Typical EDXRF spectrum for ZnS nanocrystals doped with 10% Eu impurity ions.

Table 1: Elemental analysis of Eu concentration (%) in $Zn_{1-x}Eu_xS$ nanocrystals using EDXRF technique.				Photoluminescence and Photo-Catalytic Activity of Synthesized Nanocrystals
S.N.	Nanosamples	Percentage amount of Europium present in ZnS		
		Amount of Eu added	Experimental Value	
1.	$Zn_{0.90000}Eu_{0.10000}S$	10	9.42	21
2.	$Zn_{0.99900}Eu_{0.01000}S$	1	0.96	
3.	$Zn_{0.99900}Eu_{0.00100}S$	0.1	0.14	
4.	$Zn_{0.99990}Eu_{0.00010}S$	0.01	Below detection limit	
5.	$Zn_{0.99999}Eu_{0.00001}S$	0.001	Below detection limit	

Typical EDXRF spectrum for ZnS nanocrystals doped with 10 % (at. wt. %) Eu^{3+} impurity is shown in Fig. 3. The percentage concentrations of elemental europium present in pure ZnS are given in Table 1. The analytical experimental results showed good agreement with the calculated values. However, trace amount of Ti, V and Fe impurities have been found in ZnS doped with 10% Eu^{3+} sample, whereas these impurity elements are below detection limit for all other samples. The presence of transition metal trace impurities in synthesized nanocrystals is attributed to the reported impurities in $(C_2H_3O_2)_3Eu.xH_2O$ salt.

Steady state Photoluminescence spectroscopic studies

The room temperature steady state photoluminescence spectra of $Zn_{1-x}Eu_xS$ ($0.0001 \leq x \leq 0.1$) nanocrystals have been shown in Fig. 4. PL spectra of PVP capped nanocrystals recorded at 325 nm excitation wavelength show a broad emission peak centered at 475 nm with a slight shoulder at 524 nm. Broad PL spectra attributed to the fact that the synthesized nanocrystals are not highly monodisperse. PL emission intensity increases sharply in case of ZnS nanocrystals doped with 0.01 and 0.001% Eu^{3+} ions. This shows that the dopant ions, at optimal concentrations 0.01 and 0.001%, effectively passivate the non-radiative host defect states. A strong correlation between the s-p electrons of host and the d-f electrons of dopant ions exists at appropriate concentrations of Eu^{3+} ions in the ZnS crystal lattice. It can also be imagined as the result of hybridization of electronic states, since different doping levels could result in different extents of hybridization of the electronic orbitals.

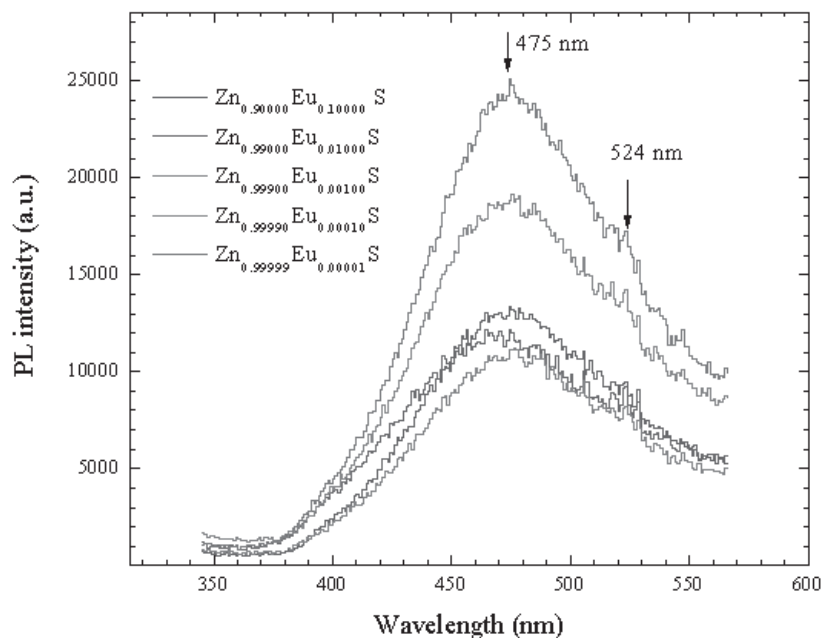


Figure 4: Room temperature PL spectra of $Zn_{1-x}Eu_xS$ ($0.0001 \leq x \leq 0.1$) nanocrystals.

It might be revealed that during synthesis process the possibility of trivalent Eu^{3+} ions to occupy any site in the ZnS lattice is quite less. This is for the reason that the ionic radius of Eu^{3+} ion (0.95 \AA) being larger than that of Zn^{2+} ion (0.74 \AA). For Eu^{3+} ion to replace a Zn^{2+} ion from its lattice site, the host lattice has to deform due to charge imbalance, which is energetically unfavorable. Therefore the position of Eu^{3+} can be (i) at the zenith of ZnS lattice co-occupied by multi-ZnS clusters; (ii) Eu^{3+} ion prefers sites with high coordination numbers and (iii) most of the Eu^{3+} ions are adsorbed on the surface of the ZnS nanocrystals. The probability of above mentioned processes depends not only on the concentration of Eu^{3+} ions, but also on the micro-crystal field around Eu^{3+} . It is worth noting that similar PL spectrum in case of Cu^{2+} doped ZnS nanocrystals has been observed by Xu et. al [5]. Moreover, many researchers [32, 33] reported PL emission in case of Eu^{3+} ions in ZnS at 590, 612, and 695 nm due to ${}^5D_0 \rightarrow {}^7F_1$, ${}^5D_0 \rightarrow {}^7F_2$ and ${}^5D_0 \rightarrow {}^7F_3$ transitions, respectively. But no such emission has been found during present measurements. This shows the possibility of reduction of $Eu^{3+} \rightarrow Eu^{2+}$ ions. Hence, the peaks centered at 475 and 524 nm may be associated with Eu^{2+} ion $4f^7-4f^65d^1$ transitions. The present PL emission is not consistent to the red emission in alkaline sulphides, because

the 5d excited states of Eu^{2+} ion are most sensitive and therefore, the $4f^65d^1$ states split due to spin-orbit coupling and crystal field [34], resulting 475 and 524 nm emissions. To investigate the aging effect, PL studies after 2 months were again performed; but there was no noticeable change in PL spectrum. This confirms the stability of synthesized nanocrystals and the possibility of dopant immigration from the host ZnS lattice.

Photo-catalytic degradation mechanism of MB dye

When a photon of UV radiation interacts with nanocrystals, dispersed in MB dye contaminated aqueous media, electrons (e^-) from valence band jumps to the conduction band leaving behind positively charged holes (h^+) in valence band. The photo-catalytic active centres are formed on the surface of $\text{Zn}_{1-x}\text{Eu}_x\text{S}$ nanocrystals due to increased negative charge in the conduction band. Actually, there are two major possibilities either photogenerated e^- and h^+ can recombine through radiative emission process or these can be trapped in defect states followed by recombination or else transferred to the nanoparticle surface where these may counter with species adsorbed on or close to the surface of the particles. The valence band holes react with the chemisorbed H_2O molecules to form reactive species such as OH^\bullet radicals whereas conduction band electrons interact with dissolved O_2 to form OH^\bullet radicals, which subsequently react with dye molecules to cause their complete degradation. Photo-catalytic efficiency of $\text{Zn}_{1-x}\text{Eu}_x\text{S}$ nanocrystals mainly depends upon amount of OH^\bullet radicals generated. Therefore, any factor that supports the generation of OH^\bullet radicals will enhance the rate of photo-catalytic degradation of MB dye. In case of Eu^{3+} doped ZnS nanocrystals, major proportion of Eu^{3+} ions may be lying on the surface of ZnS nanoparticles, which attracts conduction band electrons of ZnS nanoparticles to form the corresponding metal. These ions reduce the recombination of h^+ and e^- and hence favour the formation of OH^\bullet radicals. The photo-catalytic activity enhancing effect of Eu^{3+} ions may be explained through their ability to trap host related photoexcited electrons by acting as electron scavengers. The retardation of the electron-hole recombination will increase the photo-catalytic efficiency of the ZnS nanocrystals and, consequently, accelerate hydroxyl radical formation, which enhances the rate of MB degradation.

Fig. 5 shows schematic staging of various processes involved in photo-catalytic and photoluminescence of ZnS nanocrystals. Thermodynamically, the electron transfer from ZnS nanoparticles conduction band to the metal ions occur at the interface because the Fermi level of ZnS is higher than that of Eu. Consequently, a Schottky barrier at the Eu- ZnS contact region is formed, which improves the charge separation and enhances the photo-catalytic activity of ZnS nanocrystals.

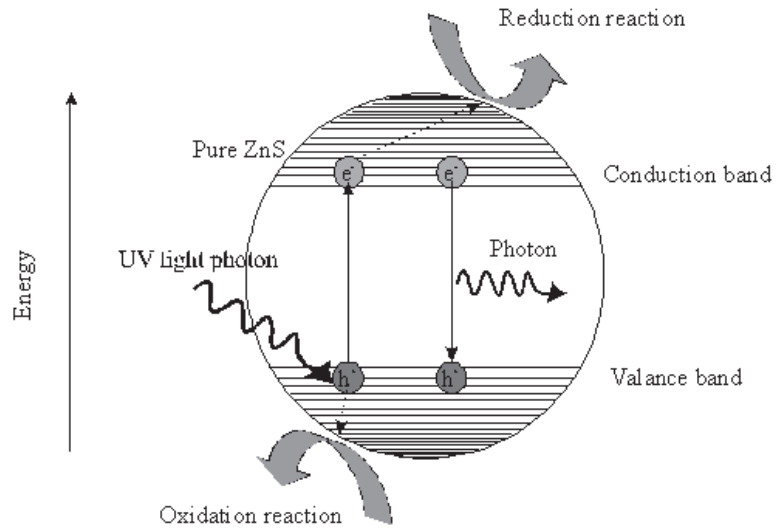


Figure 5: Schematic presentation of various processes involved in photo-catalytic and photoluminescence of ZnS nanocrystals.

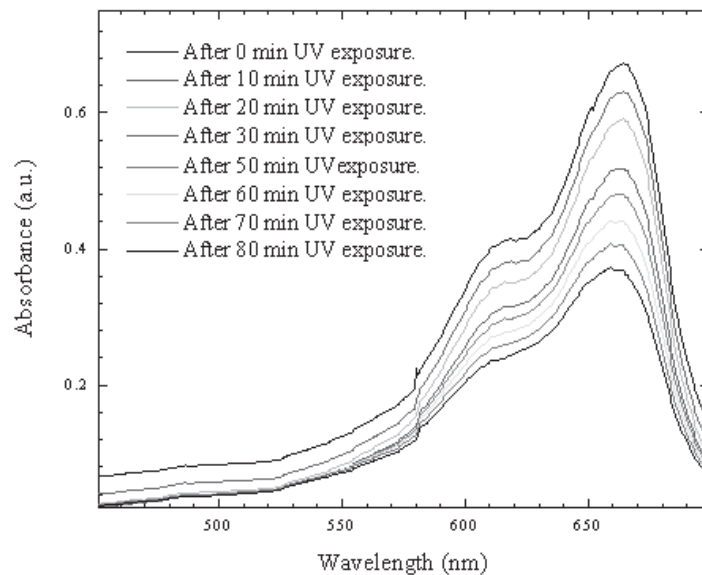


Figure 6: The absorption spectrum of MB dye in presence of Zn_{0.90000}Eu_{0.10000}S nanocrystals for different durations of UV-irradiation.

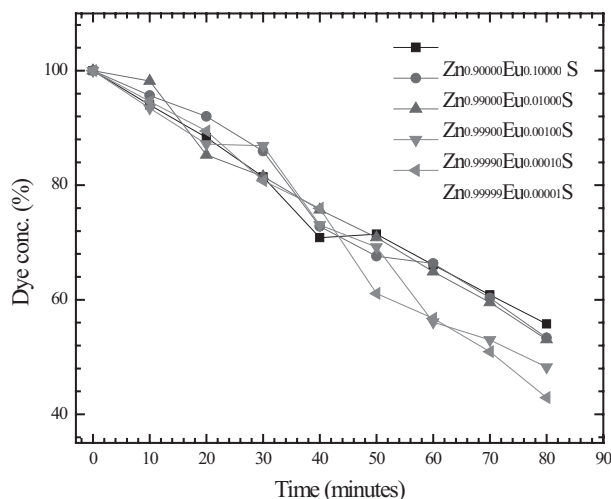


Figure 7: Photodegradation of MB dye with time in presence of $Zn_{1-x}Eu_xS$ nanocrystals.

The mentioned mechanism accorded well with the experimental results. The absorption spectra of MB dye solution for different durations of UV-irradiation in the presence of $Zn_{0.99000}Eu_{0.01000}S$ nanocrystals is shown in Fig. 6. It is clear from the Fig. 6 that the absorbance of MB dye decreases by 50% after 80 minute exposure of UV light. The sensitized photodegradation of MB dye in presence of $Zn_{1-x}Eu_xS$ ($0.0001 \leq x \leq 0.1$) nanocrystals has been plotted in Fig. 7. It has been observed that the photo-catalytic activity do not follow any regular trend. So, it has been tried to generate the linear fitted (Fig. 8) photo-catalytic curves within 5% variation of experimental results. The values of slopes for linear fitted curves are directly related with MB dye degradation or photo-catalytic activity of the nanocrystals. The variation in slopes of photo-catalytic curves with percentage of dopant concentration is shown in Fig. 9. It is evident from Fig. 9 that the values of slopes show no predicted trend for the Eu^{3+} doping; it is minimum for 1% doping and maximum for 0.001% doping concentration. Hence, $Zn_{0.99000}Eu_{0.01000}S$ nanocrystals show least photo-catalytic behavior, whereas $Zn_{0.9999}Eu_{0.00001}S$ nanocrystals have more photo-catalytic activity potential. Enhanced photo-catalytic activity at optimal Eu^{3+} concentration i.e. for $Zn_{0.9999}Eu_{0.00001}S$ nanocrystals is due to maximum probability of interfacial charge transfer by delaying the recombination of charge carriers at higher concentration. Hence the photocatalytic performance and the rate of overall quantum efficiency depend upon the competition between the charge carrier recombination and charge carrier trapping followed by the competition between recombination of trapped carriers and interfacial charge transfer.

Chitkara, M.
Kumar, K.
Singh, K.
Kumar, S.
Sandhu, I. S.

26

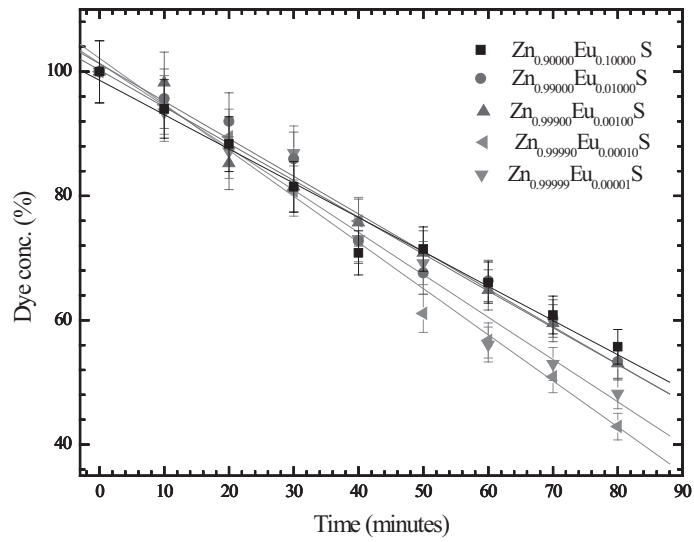


Figure 8: Linear fitted photodegradation curves of MB dye in presence of Zn_xEu_xS nanocrystals.

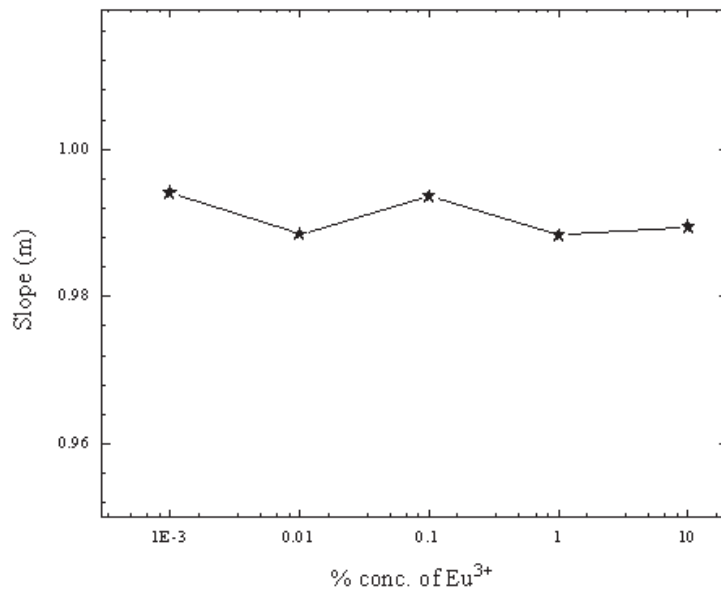


Figure 9: Variation of linear fitted slopes for photodegradation curves vs. dopant concentration.

CONCLUSIONS

Wet chemical co-precipitation method is an eco-friendly facile synthesis technique, which gives good yield of PVP capped $Zn_{1-x}Eu_xS$ ($0.00001 \leq x \leq 0.1$) nanocrystals. XRD and TEM studies reveal that synthesized nanoparticles are single nanocrystals having average size ~ 3 nm. Both, photo-catalytic and photoluminescence studies show dopant concentration dependence at optimal concentrations. The broad PL peak centred at 475 nm overlapped with a weak peak at 524 nm may be attributed to $4f^7-4f^65d^1$ radiative transitions of dopant ions due to reduction of $Eu^{3+} \rightarrow Eu^{2+}$. These non-toxic, stable, inexpensive nano-photocatalysts having high redox potentials can be efficiently used for environmental cleaning, water purification and H_2 production. Moreover, linear fitted photo-catalytic curves and PL spectra reported in the present investigation will be very beneficial for future applications of these nanocrystals in opto-electronic industry.

27

ACKNOWLEDGEMENTS

The Regional Scientific Instruments Centre (RSIC), Punjab University, Chandigarh is gratefully acknowledged for XRD and TEM studies. The authors would like to thank Dr. Devinder Mehta, Professor, Department of Physics, Panjab University, Chandigarh for the use of EDXRF facility. Authors are highly thankful to Dr. Sanjiv Aggarwal, associate Professor, Department of Physics, Kurukshetra University, Kurukshetra for energy resolved spectroscopic studies and fruitful discussions.

REFERENCES

- [1] J.I. Brauman, *Science* **271** (1996) 889. <http://dx.doi.org/10.1126/science.271.5251.889>
- [2] L.E. Brus, *J. Phys. Chem.* **90** (1986) 2555. <http://dx.doi.org/10.1021/j100403a003>
- [3] L.D. Sun, X.F. Fu, M.W. Wang, C.H. Liu, C.H. Liao, C.H. Yan, *J. Lumin.* **87** (2000) 538. [http://dx.doi.org/10.1016/S0022-2313\(99\)00283-5](http://dx.doi.org/10.1016/S0022-2313(99)00283-5)
- [4] A.A. Khosravi, M. Kundu, L. Jatwa, S.K. Deshpande, U.A. Bhagwat, M. Sastry, S. K. Kulkarni, *Appl. Phys. Lett.* **67** (1995) 2702. <http://dx.doi.org/10.1063/1.114298>
- [5] S.J. Xu, S.J. Chua, B. Liu, L.M. Gan, C.H. Chew, G.Q. Xu, *Appl. Phys. Lett.* **73** (1998) 478. <http://dx.doi.org/10.1063/1.121906>
- [6] M. Bruchez, M. Moronne, P. Gin, S. Weiss, A.P. Alivisatos, *Science* **281** (1998) 2013. <http://dx.doi.org/10.1126/science.281.5385.2013>
- [7] Y.W. Cao, U. Banin, *Angew. Chem. Int. Ed. Engl.* **38** (1999) 3692. [http://dx.doi.org/10.1002/\(SICI\)1521-3773\(19991216\)38:24<3692::AID-ANIE3692>3.0.CO;2-W](http://dx.doi.org/10.1002/(SICI)1521-3773(19991216)38:24<3692::AID-ANIE3692>3.0.CO;2-W)
- [8] M.F. Garcia, A.M. Arias, J.C. Hanson, J.A. Rodriguez, *Chem. Rev.* **104** (2004) 4063. <http://dx.doi.org/10.1021/cr030032f>
- [9] I. Gur, N.A. Fromer, M.L. Geier, A.P. Alivisatos, *Science* **310** (2005) 462. <http://dx.doi.org/10.1126/science.1117908>
- [10] R.N. Bhargava, D. Gallagher, X. Hong, A. Nurmikko, *Phys. Rev. Lett.* **72** (1994) 416. <http://dx.doi.org/10.1103/PhysRevLett.72.416>
- [11] C. Sihal, I. Takashi, K. Keisaku, *J. Phys. Chem. B* **102** (1998) 6169. <http://dx.doi.org/10.1021/jp9809991>

Chitkara, M.
Kumar, K.
Singh, K.
Kumar, S.
Sandhu, I. S.

- [12] K. Singh, N.K. Verma, H.S. Bhatti, *Physica B: Condensed Matter* **402** (2009) 300. <http://dx.doi.org/10.1016/j.physb.2008.10.058>
- [13] K. Singh, S. Kumar, N.K. Verma, H.S. Bhatti, *J. Nanopart. Res.* **11** (2009) 1017. <http://dx.doi.org/10.1007/s11051-009-9586-1>
- [14] M.R. Hoffmann, S.T. Martin, W. Choi, D.W. Bahnemann, *Chem. Rev.* **95** (1995) 69. <http://dx.doi.org/10.1021/cr00033a004>
- [15] M. Anpo, M. Takeuchi, *J. Catal.* **216** (2003) 205. [http://dx.doi.org/10.1016/S0021-9517\(02\)00104-5](http://dx.doi.org/10.1016/S0021-9517(02)00104-5)
- [16] I.N. Martyanov, E.N. Savinov, K.J. Klabunde, *J. Colloid Interface Sci.* **111** (2003) 267. [http://dx.doi.org/10.1016/S0021-9797\(03\)00678-7](http://dx.doi.org/10.1016/S0021-9797(03)00678-7)
- [17] A.M. Ali, E.A. Emanuelsson, D.A. Patterson, *Appl. Catal. B* **168** (2010) 98. <http://dx.doi.org/10.1155/2013/234806>
- [18] S.K. Pardeshi, A.B. Patil, *J. Mol. Catal. A: Chem.* **32** (2009) 308. <http://dx.doi.org/10.1016/j.molcata.2009.03.023>
- [19] S. Baruah, M.A. Mahmood, M.T. Myint, T. Bora, J. Dutta, *Beilstein J. Nanotechnol.* **14** (2010) 1. <http://dx.doi.org/10.3762/bjnano.1.3>
- [20] S. Colis, H. Bieber, S.B. Colin, G. Schmerber, C. Leuvrey, A. Dinia, *Chem. Phys. Lett.* **529** (2006) 422. <http://dx.doi.org/10.1016/j.cplett.2006.02.109>
- [21] R. Ullah, J. Dutta, *J. Hazard. Mater.* **194** (2008) 156. <http://dx.doi.org/10.1016/j.jhazmat.2007.12.033>
- [22] R. Wang, J.H. Xin, Y. Yang, H. Liu, L. Xu, J. Hu, *Appl. Surf. Sci.* **312** (2004) 227. <http://dx.doi.org/10.1016/j.apsusc.2003.12.012>
- [23] Y. Zheng, C. Chen, Y. Zhan, X. Lin, Q. Zheng, K. Wei, J. Zhu, Y. Zhu, *Inorg. Chem.* **46** (2007) 6675. <http://dx.doi.org/10.1021/ic062394m>
- [24] C.C. Wang, Z. Zhang, J.Y. Ying, *Nanostruct. Mater.* **9** (1997) 583. [http://dx.doi.org/10.1016/S0965-9773\(97\)00130-X](http://dx.doi.org/10.1016/S0965-9773(97)00130-X)
- [25] W. Choi, A. Termin, R.M. Hoffmann, *J. Phys. Chem.* **98** (1994) 13669. <http://dx.doi.org/10.1021/j100102a038>
- [26] J.S. Hu, L.L. Ren, T.G. Guo, H.P. Liang, A.M. Cao, L.J. Wan, C.L. Bai, *Angew. Chem. Int. Ed.* **44** (2005) 1269. <http://dx.doi.org/10.1002/anie.200462057>
- [27] J.H. Bang, R.J. Helmich, K.S. Suslick, *Adv., Mater.* **20** (2008) 2599. <http://dx.doi.org/10.1002/adma.200703188>
- [28] V. Albe, C. Jouanin, D. Bertho, *Phys. Rev. B* **57** (1998) 8778. <http://dx.doi.org/10.1103/PhysRevB.57.8778>
- [29] S. Lingdong, Y. Chunhua, L. Changhui, L. Chunsheng, L. Dan, Y. Jiaqi, *J. Alloys Compounds* **275** (1998) 234. [http://dx.doi.org/10.1016/S0925-8388\(98\)00310-7](http://dx.doi.org/10.1016/S0925-8388(98)00310-7)
- [30] S.C. Qu, W.H. Zhou, F.Q. Liu, N.F. Chen, Z.G. Wang, H.Y. Pan, D.P. Yu, *Appl. Phys. Lett.* **80** (2002) 3605. <http://dx.doi.org/10.1063/1.1478152>
- [31] B.D. Cullity, *Elements of X-ray diffraction*, Addison-Wesley, Massachusetts 1978 p. 102.
- [32] D.D. Papakonstantinou, J. Huang, P. Lianos, *J. Mat. Sci. Lett.* **17** (1998) 1571. <http://dx.doi.org/10.1023/A:1006543205507>
- [33] W. Chen, J.O. Malm, V. Zwiller, Y. Huang, S. Liu, R. Wallenberg, J.O. Bovin, L. Samuelson, *Phys. Rev. B* **61** (2000) 11021. <http://dx.doi.org/10.1103/PhysRevB.61.11021>
- [34] S.M. Liu, H.Q. Guo, Z.H. Zhang, F.Q. Liu, Z.G. Wang, *Chin. Phys. Lett.* **17** (2000) 609. <http://dx.doi.org/10.1088/0256-307X/17/8/023>